Eleven-vertex Polyhedral Monocarbaplatinaborane Chemistry. Structure and Fluxionality of [8,8-$(PMe_2Ph)_2$-*nido*-8,7-$PtCB_9H_{11}$]*

Bohumil Štíbr,[a] Tomáš Jelínek,[a] John D. Kennedy,[b] Xavier L. R. Fontaine[b] and Mark Thornton-Pett[b]

[a] *Institute of Inorganic Chemistry, The Academy of Sciences of the Czech Republic, 25068 Řež, The Czech Republic*

[b] *School of Chemistry, University of Leeds, Leeds LS2 9JT, UK*

Reaction between $[PtCl_2(PMe_2Ph)_2]$ and [*arachno*-6-$CB_9H_{14}]^-$ in CH_2Cl_2 solution at room temperature yields yellow air-stable eleven-vertex [8,8-$(PMe_2Ph)_2$-*nido*-8,7-$PtCB_9H_{11}$] **1** (46–64%) together with small quantities of ten-vertex [9,9-$(PMe_2Ph)_2$-*arachno*-9,6-$PtCB_8H_{12}$] **2** (0–3%). Crystals of compound **1** are monoclinic, space group $P2_1/n$, with a = 1186.8(1), b = 1554.1(2), c = 1344.1(2) pm, β = 95.02(1)° and Z = 4. The structure refined to R, R' = 0.0297, 0.0310 using 3938 data with $I > 3\sigma(I)$. The cluster structure is of the *nido* eleven-vertex type, with the platinum and carbon atoms occupying adjacent positions on the open face. There is some geometrical closure from pure *nido*, so that the gross cluster structure tends towards intermediacy between those of [7,7-$(PMe_2Ph)_2$-*nido*-7-$PtB_{10}H_{12}$] **4** and of the *closo*-structured species [1,1-$(PMe_2Ph)_2$-1,2,3-$PtC_2B_8H_{10}$] **3**. The NMR properties of **1** are reported and assessed for intermediacy between those of **3** and **4**, and the analytical utility of NMR spectroscopy in assessing the metal-to-cluster bonding is developed by comparison with non-metallated species. The metal-to-carborane bonding sphere of compound **1** is fluxional, with $\Delta G^{\ddagger}_{313}$ *ca.* 62 kJ mol^{-1}. The fluxional process involves an interconversion of enantiomers with the platinum centre and the bridging hydrogen atom migrating around the open face of the $\{CB_9H_{10}\}$ cage while the $\{(PMe_2Ph)_2\}$ exo polyhedral ligand sphere undergoes a half-twist.

There are intriguing structural variations within the eleven-vertex boron-containing polyhedral systems that have *pileo*, *closo* or *nido* formal cluster-electron counts.[1-3] Recently we have presented work on dicarbaplatinaundecaborane systems, based on [1,1-$(PMe_2Ph)_2$-1,2,3-$PtC_2B_8H_{10}$] **3**, which are of closed configuration **I**.[3] In compound **3** the closed cluster structure differs from that exhibited by its ostensibly isoelectronic (non-carba-)platinaundecaborane analogue [7,7-$(PMe_2Ph)_2$-*nido*-7-$PtB_{10}H_{12}$] **4** which has an essentially straightforward open *nido* cluster geometry **III**.[4] Each of compounds **3** and **4** exhibits a different rotational fluxional behaviour in the metal-to-cluster binding mode.[3-5]

In this context it was of interest to attempt to prepare the previously unreported intermediate isoelectronic monocarbaplatinaundecaborane [8,8-$(PMe_2Ph)_2$-*nido*-8,7-$PtCB_9H_{11}$] **1** to examine it for intermediacy of structural behaviour (schematic structure **II**), for intermediacy of fluxional behaviour, and for intermediacy of electronic structure as manifested in comparative NMR properties.

The numbering systems used in this work are in structures **IV** (ten-vertex *nido*/*arachno* type), **V** (eleven-vertex *nido* type), and **VI** (eleven-vertex *closo* type). Interconversion among these structural types generally changes the formal numbering of a given atom (*e.g.* Fig. 4 below).

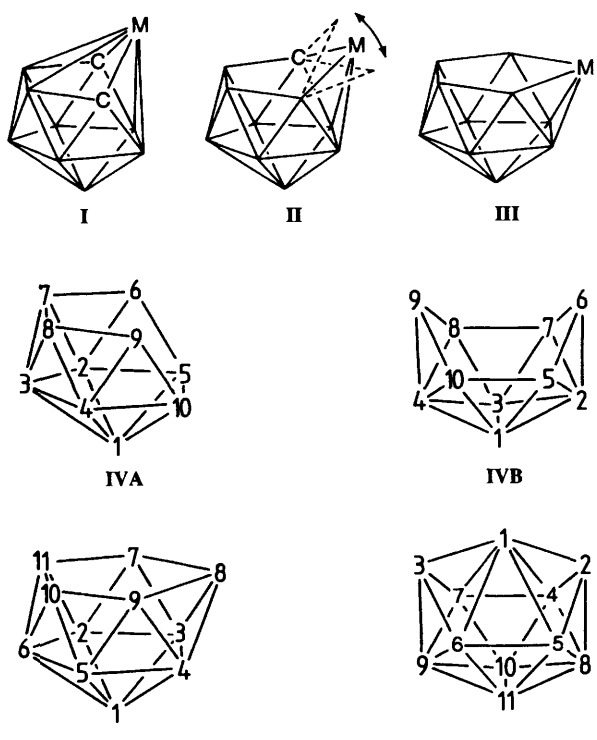

Results and Discussion

Preparation of [8,8-$(PMe_2Ph)_2$-*nido*-8,7-$PtCB_9H_{11}$] **1**.—The reaction between Cs[*arachno*-6-CB_9H_{14}][6] and *cis*-$[PtCl_2(PMe_2Ph)_2]$ in dichloromethane solution at room temperature for 24 h, followed by chromatographic separation, yielded two monocarbametallaborane products in sufficient yield (reaction scale *ca.* 250 μmol) for further characterisation. Trace quantities of other yellow polyhedral boron-containing compounds were present, but these were uncharacterisable on the scale obtained. The major product (46–64% yield) was [8,8-$(PMe_2Ph)_2$-*nido*-8,7-$PtCB_9H_{11}$] **1**, a yellow air-stable crystalline solid, identified

* *Supplementary data available:* see Instructions for Authors, *J. Chem. Soc., Dalton Trans.*, 1993, Issue 1, pp. xxiii–xxviii.

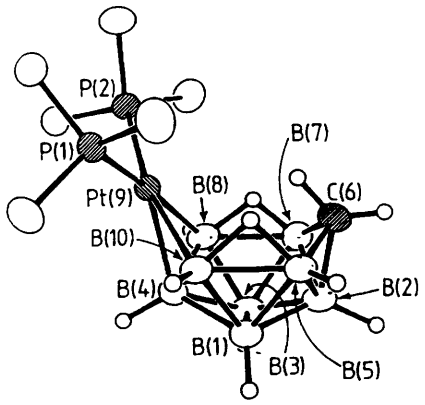

Fig. 1 An ORTEP-type drawing[7] of the molecular structure of [9,9-$(PMe_2Ph)_2$-*arachno*-9,6-$PtCB_8H_{12}$] **2**; data from ref. 8

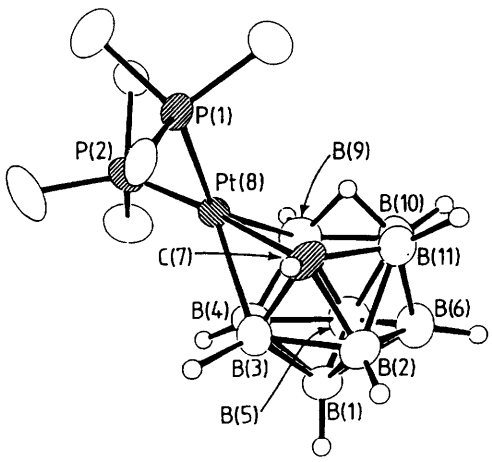

Fig. 2 An ORTEP-type drawing of the crystallographically determined solid-state molecular structure of [8,8-$(PMe_2Ph)_2$-*nido*-8,7-$PtCB_9H_{11}$] **1**, with phosphine carbon atoms, except for those bound directly to phosphorus, omitted for clarity

and characterised as described below. The reaction proceeded readily in the absence of base [equation (1)].

$$[PtCl_2(PMe_2Ph)_2] + [CB_9H_{14}]^- \longrightarrow [(PMe_2Ph)_2PtCB_9H_{11}] + Cl^- + H_2 + HCl \quad (1)$$

The second most abundant product (0–3% yield) was the very pale yellow, air-stable, ten-vertex compound [9,9-$(PMe_2Ph)_2$-*arachno*-9,6-$PtCB_8H_{12}$] **2** (Fig. 1). Compound **2** is (to be) described elsewhere[8] as part of the *arachno* ten-vertex series [9,9-$(PMe_2Ph)_2$-*arachno*-9,6-$PtEB_8H_{10}$] (E = CH_2, NH or S) prepared by more direct syntheses.

Molecular Structure of [8,8-$(PMe_2Ph)_2$-*nido*-8,7-$PtCB_9H_{11}$] **1**.—The crystal and molecular structure of compound **1** was determined by single-crystal X-ray diffraction analysis, which confirmed it as [8,8-$(PMe_2Ph)_2$-*nido*-8,7-$PtCB_9H_{11}$] (Fig. 2 and Tables 1 and 2). All cluster hydrogen atoms were located and refined.

The monocarbamonometallaborane has a *nido* eleven-vertex cluster geometry, but with a substantial tilt of the Pt(8) vertex out of the planar open face (see below near Table 3 and Fig. 3). The carbon atom C(7) is on the open face adjacent to this platinum vertex, and there is an open-face hydrogen bridge at the B(9)–B(10) site, equivalent to one of the bridging positions in the previously described[4] non-carbon analogue [7,7-$(PMe_2Ph)_2$-*nido*-7-$PtB_{10}H_{12}$] **4**. Compounds **1** and **4** are in the first instance related by the replacement of the C(7) carbon atom in **1** by a boron atom together with a hydrogen atom bridging to the next adjacent boron atom [B(11) in Fig. 2] on the open face of **4**.

Table 1 Selected interatomic distances (pm) for [8,8-$(PMe_2Ph)_2$-*nido*-8,7-$PtCB_9H_{11}$] **1** with estimated standard deviations (e.s.d.s) in parentheses

(*i*) From the metal atom			
Pt(8)–P(1)	234.3(3)	Pt(8)–P(2)	226.0(3)
Pt(8)–B(3)	226.2(8)	Pt(8)–B(4)	224.5(8)
Pt(8)–C(7)	218.7(7)	Pt(8)–B(9)	228.4(8)
(*ii*) Carbon–boron			
C(7)–B(2)	168.0(10)	C(7)–B(3)	160.0(10)
C(7)–B(11)	157.0(11)		
(*iii*) Boron–boron			
B(1)–B(2)	174.9(11)	B(1)–B(5)	178.0(12)
B(1)–B(3)	173.2(12)	B(1)–B(4)	177.6(11)
B(1)–B(6)	180.8(11)		
B(2)–B(3)	173.0(11)	B(4)–B(5)	176.7(12)
B(2)–B(6)	174.3(12)	B(5)–B(6)	180.4(12)
B(2)–B(11)	179.7(11)	B(5)–B(10)	173.5(11)
B(3)–B(4)	186.1(11)		
B(4)–B(9)	178.8(10)	B(5)–B(9)	170.2(11)
B(6)–B(10)	173.8(12)	B(6)–B(11)	175.1(10)
B(10)–B(11)	193.3(11)		
(*iv*) Phosphorus–carbon			
P(1)–C(11)	180.6(7)	P(2)–C(21)	181.1(7)
P(1)–C(12)	182.2(7)	P(2)–C(22)	182.0(8)
P(1)–C(131)	181.1(5)	P(2)–C(231)	180.1(5)

The $\{Pt(PMe_2Ph)_2\}$ unit is twisted away from a reference plane through Pt(8)B(1)B(6), the dihedral angle Φ between Pt(8)P(1)P(2) and C(7)Pt(8)B(9) being 36.5(2)°. There is a similar twist in [7,7-$(PMe_2Ph)_2$-*nido*-7-$PtB_{10}H_{12}$] **4** in the solid state,[4] but since this unit in compounds **1** and **4** is fluxionally bound to the polyhedral residue in solution (see below) it is not certain whether the observed solid-state configurations represent the minimum-energy fluxional conformers. In compound **1**, however, the P(2) atom is almost exactly *trans* to C(7) [P(2)–Pt(8)–C(7) 175.9(2)°], suggesting, in terms of a square-planar dsp^2-type platinum(II) description (see NMR section below), that there may be directive contributions from Pt(8)–C(7) two-centre two-electron character *trans* to P(2), with P(1) thereby being *trans* to a three-centre Pt(8)B(4)B(9) interaction. Additional dp-type platinum-orbital participation could be invoked for the close approach of the B(3) atom to platinum (compare refs. 4, 5, 9–11 and 12).

Compound **1** can be examined for intermediacy of structure (see **II**) between the conventionally[13,14] *nido* compound **4** (structure **III**)[4] and closed compound **3** (structure **I**).[3] Relevant dimensions are in Table 3, and appropriate views of the clusters are in Fig. 3. The angles θ correspond to the angle between the {Pt(8)C(7)B(9)} and {B(2)B(5)C(7)B(9)} planes in compound **1** (Fig. 2), and are convenient for the comparison; θ is zero for the symmetrical closed structure of compound **3**.

The data for compound **1** indicate some shift from the *nido* structure of compound **4** towards the closed structure of compound **3** and suggest a corresponding structural continuum in the $\{PtB_{10}H_{12}\} \longrightarrow \{PtCB_9H_{11}\} \longrightarrow \{PtC_2B_8H_{10}\}$ cluster sequence. However, inspection of the detailed dimensions (Table 3) shows that the shift of compound **1** towards closed is not marked, and that, in geometrical terms, much of the open *nido* character remains.

Comparative NMR Studies.—It is of interest to see how these structural considerations are reflected in electronic structure. Since NMR nuclear shielding depends upon electronic structure, the assigned ^{11}B NMR shielding patterns for compounds **1**, **3**

Table 2 Selected angles (°) between interatomic vectors for compound **1** with e.s.d.s in parentheses

(i) About the metal atom			
P(1)–Pt(8)–P(2)	95.6(2)	P(2)–Pt(8)–B(4)	97.4(3)
P(1)–Pt(8)–B(3)	114.9(3)	P(2)–Pt(8)–B(3)	134.2(2)
P(1)–Pt(8)–B(4)	163.6(2)	P(2)–Pt(8)–B(9)	91.1(3)
P(1)–Pt(8)–C(7)	85.8(2)	P(2)–Pt(8)–C(7)	175.9(2)
P(1)–Pt(8)–B(9)	143.2(2)	C(7)–Pt(8)–B(9)	90.1(3)
B(3)–Pt(8)–B(4)	48.8(2)	B(4)–Pt(8)–B(9)	46.5(2)
B(3)–Pt(8)–C(7)	42.1(2)	B(4)–Pt(8)–C(7)	80.6(3)
B(3)–Pt(8)–B(9)	84.2(3)		
(ii) About the cage carbon atom			
Pt(8)–C(7)–B(2)	126.2(5)	B(11)–C(7)–B(3)	114.7(6)
Pt(8)–C(7)–B(3)	71.5(4)	B(11)–C(7)–B(2)	67.1(5)
Pt(8)–C(7)–B(11)	110.4(5)	B(2)–C(7)–B(3)	63.6(5)
(iii) Boron–boron–platinum			
B(1)–B(3)–Pt(8)	116.5(5)	B(1)–B(4)–Pt(8)	115.5(5)
B(2)–B(3)–Pt(8)	119.3(5)	B(5)–B(4)–Pt(8)	114.6(4)
B(4)–B(3)–Pt(8)	65.1(4)	B(3)–B(4)–Pt(8)	66.1(4)
B(5)–B(4)–Pt(8)	114.6(4)	B(9)–B(4)–Pt(8)	67.9(4)
(iv) Boron–boron–carbon			
B(1)–B(2)–C(7)	104.5(5)	B(1)–B(3)–C(7)	108.9(6)
B(3)–B(2)–C(7)	55.9(4)	B(2)–B(3)–C(7)	60.4(4)
B(6)–B(2)–C(7)	102.8(5)	B(4)–B(3)–C(7)	111.7(5)
B(11)–B(2)–C(7)	53.5(4)		
B(2)–B(11)–C(7)	59.4(5)	B(6)–B(11)–C(7)	107.6(3)
B(10)–B(11)–C(7)	114.6(5)		
(v) Carbon–phosphorus–platinum			
C(11)–P(1)–Pt(8)	109.2(3)	C(21)–P(2)–Pt(8)	117.8(3)
C(12)–P(1)–Pt(8)	124.7(3)	C(22)–P(2)–Pt(8)	109.9(3)
C(131)–P(1)–Pt(8)	110.4(2)	C(231)–P(2)–Pt(8)	115.4(2)
(vi) Others			
B–B–B(acute)		56.7(5)–67.3(5)	
B–B–B(obtuse)		103.2(5)–118.6(6)	
C–P–C		101.3(4)–108.1(4)	

and **4** provide a criterion. An NMR comparison of the $\{CB_9H_{11}\}$ carborane ligand fragment with the *nido*[15] and *arachno*[4,16] anions $[6\text{-}CB_9H_{12}]^-$ and $[6\text{-}CB_9H_{14}]^-$ is also informative.

For geometrically *nido* $[7,7\text{-}(PMe_2Ph)_2\text{-}nido\text{-}7\text{-}PtB_{10}H_{12}]$ **4** the $\eta^4\text{-}\{B_{10}H_{12}\}$ NMR properties[17] have suggested an essentially *nido*-decaboranyl structure, but with some *arachno* character in the $\eta^4\text{-}\{B_4\}$ region bound to platinum.[5,11,12,17,18] On the other hand, for geometrically *closo* $[1,1\text{-}(PMe_2Ph)_2\text{-}1,2,3\text{-}PtC_2B_8H_{10}]$ **3** the NMR properties of the $\eta^6\text{-}\{C_2B_8H_{10}\}$ unit are closer[3,19] to those of *arachno*-$C_2B_8H_{14}$; by contrast, in closely related $[1,1\text{-}(SEt_2)_2\text{-}closo\text{-}1,2,3\text{-}PtC_2B_8H_{10}]$ **5** the same unit exhibits intermediate *nido*/*arachno* behaviour.[3,19]

The ^{11}B and ^1H NMR resonances for compound **1** (Table 4) were assigned by the incidence of ^{195}Pt satellites, and by $[^{11}B\text{–}^{11}B]$-[20,21] and $[^1H\text{–}^1H]$-COSY (correlation spectroscopy)[22] experiments. Because of fluxionality at higher temperatures (see below), the static form discussed here was examined at *ca.* 273 K. In the interproton COSY spectrum, for which ^2J and ^3J pathways generally predominate in polyhedral boron chemistry,[22] there was an abnormally high incidence of formal $^4J(^1H\text{–}^1H)$ cross-peaks,* presumably from exchange correlation arising from fluxionality (see below). Interproton COSY NMR experiments at lower temperatures should in principle not show such exchange-correlation cross-peaks, but the lower solubility of compound **1** at lower temperatures engendered impractically long acquisition times for this. Conversely, however, the recognition of the fluxionality mechanism, and the concomitant identification of the pairs of exchanging sites, confirmed the ^{11}B and ^1H assignments.

Table 3 Selected comparative dimensions (using numbering scheme of **1**) for the $\{PtCB_9\}$ compound **1** (this work), the $\{PtB_{10}\}$ compound **4** (ref. 4) and $\{PtC_2B_8\}$ compound **3** (ref. 3)

	1	**4**	**3**
Distances (pm)			
Pt(8)–B(3)	226.2(8)	221.4(5)	237.4(6)
Pt(8)–B(4)	224.5(8)	222.5(6)	237.5(6)
Pt(8)–C(7)	218.7(7)	227.9(6)	217.6(5)
Pt(8)–B(9)	228.4(8)	230.0(6)	218.5(4)
Pt(8)–B(10)	326.8(7)	341.9(6)	238.3(5)
Pt(8)–B(11)	310.6(7)	345.9(6)	240.1(4)
Dihedral angles (°)			
Pt(8)B(9)C(7)/P(1)Pt(8)P(2)	143.5(2)	144.4(2)	94.8(1)
Pt(8)B(9)C(7)/B(3)B(4)C(7)B(9)	81.7(2)	77.6(2)	108.2(2)
Pt(8)B(9)C(7)/C(7)B(9)B(10)B(11)	153.3(2)	163.1(2)	110.2(2)
Pt(8)B(9)C(7)/B(2)B(5)C(7)B(9)	36.6(2)	42.6(2)	1.0(2)

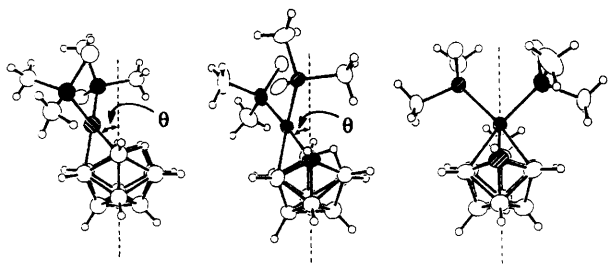

Fig. 3 ORTEP-type drawings of the cluster $\{PtB_{10}\}$, $\{PtCB_9\}$ and $\{PtC_2B_8\}$ units of (from left to right) compounds **4**, **1** and **3** respectively, illustrating the progressive closure from *nido*-type geometry in **4** to *closo*-type in **3** (data from this work, and refs. 3 and 4). In compounds **4**, **1** and **3** the angle θ is respectively 43, 37 and 0°. For an eleven-vertex fragment of a regular triangulated icosahedron it would be 62°

Fig. 4 compares the shielding patterns among compound **1** and non-metallated *nido* and *arachno* $[6\text{-}CB_9H_{12}]^-$ and $[6\text{-}CB_9H_{14}]^-$. This permits assessment of the character of the $\{CB_9H_{11}\}$ cluster when bound to $\{Pt(PMe_2Ph)_2\}$, to see if it better resembles a *nido* or *arachno* fragment. This in turn permits the assessment of whether compound **1** is formally best regarded as an effective platinum(II) complex of $\{nido\text{-}CB_9H_{11}\}^{2-}$, or as an effective platinum(IV) complex of $\{arachno\text{-}CB_9H_{11}\}^{4-}$, or as having intermediate character. Compared to the *nido* anion, compound **1** shows a small decrease in overall shielding [mean $\delta(^{11}B)$ −4.4 for **1** and −9.1 for the anion], but the sequence of ^{11}B shielding is approximately the same except for B(9) (α to platinum) and B(10) (β to platinum) that bind the face-bridging hydrogen. In particular, compound **1** retains higher shielding at B(2) and B(5) [corresponding to *nido* ten-vertex B(2) and B(4)], which is a general *nido* ten-vertex feature. By contrast, $[arachno\text{-}6\text{-}CB_9H_{14}]^-$ has a higher overall shielding [$\delta(^{11}B)$ (mean) −22.1], characteristic of a ten-vertex *nido* ⟶ *arachno* difference.[23,24] Additionally, compared to compound **1**, there is a crossover to $^{11}B(2,4)$ at lowest and $^{11}B(1,3)$ at highest shielding, also a characteristic of a ten-vertex *nido* ⟶ *arachno* change.[23,24] These considerations and the trends in Fig. 4 therefore suggest that the $\{CB_9H_{11}\}$ fragment in compound **1**, although exhibiting some intermediate character, has more similarities to $[nido\text{-}CB_9H_{12}]^-$ than to the starting *arachno* ten-vertex substrate. The formal metal-to-carborane bonding could therefore in the first instance be regarded in terms of a platinum(II) complex between $\{Pt(PMe_2Ph)_2\}^{2+}$ and bidentate *tetrahapto* $\{nido\text{-}CB_9H_{11}\}^{2-}$, with a basic two-orbital

* Note that superscripts *n* in ^nJ for polyhedral borane species refer to the number of edge connectors between the two atoms in question, and do not necessarily imply *n* two-electron two-centre bonds as is usually the case in other areas of chemistry.

Table 4 Cluster ^{11}B and ^{1}H NMR data for [8,8-$(PMe_2Ph)_2$-*nido*-8,7-$PtCB_9H_{11}$] **1** in CD_2Cl_2 solution at 273 K

Assignment	$\delta(^{11}B)$	Observed [^{11}B–^{11}B] COSY correlations[a,b]	$\delta(^{1}H)$	Observed [^{1}H–^{1}H] COSY correlations[b,c]
1	−11.0[d]	2s 5s	+1.55[e]	5m
2	−23.8	1s 6w	+2.00[f]	3w? 6w 7m, 11w
3	+9.3[d]	—	+2.90	4w? 7w $11w^4$
4	−4.2[d,g]	1 vw?	+2.04	3w? $6w^4$ $10w^4$
5	−15.4	1s 6w 10w	+2.22	1m 6m 9m 10m μm
6	+1.6[d]	2w 5w 10w	+2.54	2w $4w^4$ 5m 10w μm
7	[CH]	—	+3.94[h]	2s 3w 11m
9	+7.9	—	+3.07	5s μs^2
10	−18.1[d]	5w 6w	+1.29	$4w^4$ 5m 6w μs^2
11	+9.9[d]	—	+3.41	2w $3w^4$ 7m
μ(9,10)	—	—	−1.27[i]	5m 5m $9s^2$ $10s^2$

[a] From {^{1}H(broad-band decoupled)} experiment. [b] s = Strong, m = intermediate, w = weak. [c] From {^{11}B(broad-band decoupled)} experiment; numerical superscripts refer to ^nJ coupling pathway when $n \neq 3$. The apparent high incidence of ^4J pathways probably arises from exchange correlation. [d] Coalescence in pairs (1,6), (4,10) and (3,11) observed at 332–340 K ($C_2D_2Cl_4$ solution, 9.4 T). [e] $^3J(^{195}Pt$–$^{1}H)$ 37 Hz. [f] $^3J(^{195}Pt$–$^{1}H)$ 58 Hz. [g] $^1J(^{195}Pt$–$^{11}B)$ *ca.* 150 Hz. [h] $^2J(^{195}Pt$–$^{1}H)$ 31; $^3J(^{31}P$–$^{1}H)$ (*trans*) 16 Hz; *trans* coupling to $^{31}P(2)$ established by ^{1}H-{^{31}P(selective)} experiment. [i] Sharpened by ν[$^{11}B(10)$] much more than by ν[$^{11}B(9)$] in ^{1}H-{^{11}B(selective)} experiments.

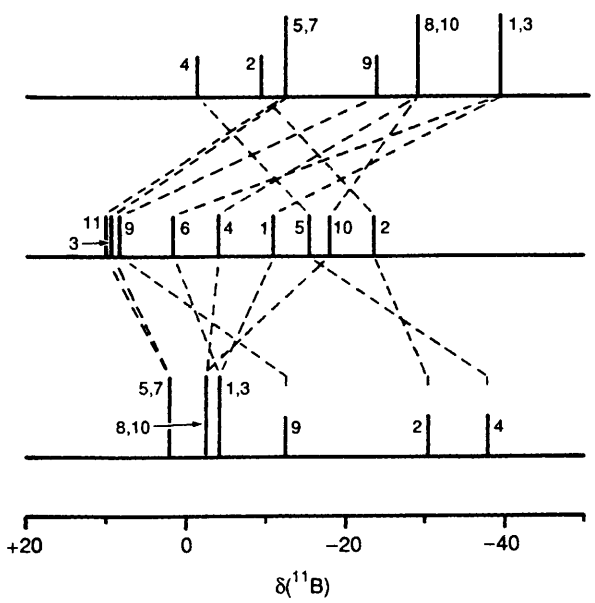

Fig. 4 Stick diagrams of the chemical shifts and relative intensities in the ^{11}B NMR spectra of, from top to bottom, [*arachno*-6-CB_9H_{14}]$^-$, compound **3**, and [*nido*-6-CB_9H_{10}]$^-$, with hatched lines joining equivalent positions for the three species. The characteristic [*nido*-6-CB_9H_{10}]$^-$ ⟶ [*arachno*-6-CB_9H_{14}]$^-$ crossover from low to high shielding for the 1,3 positions and from high to low shielding for the 2,4 positions occurs in the **3** ⟶ [CB_9H_{14}]$^-$ shielding changes rather than the [CB_9H_{10}] ⟶ **3** changes

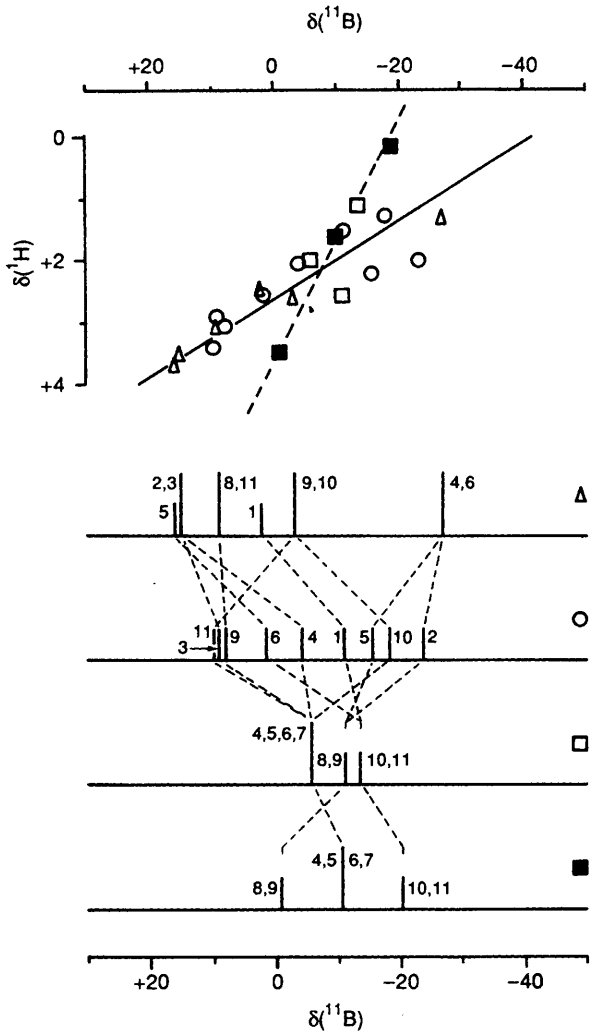

Fig. 5 Representations of selected NMR data for closed [1,1-$(PMe_2Ph)_2$-1,2,3-$PtC_2B_8H_{10}$] **3** [■, $\delta(^{11}B)$ (mean) −11.1], closed [1,1-$(SEt_2)_2$-1,2,3-$PtC_2B_8H_{10}$] [**5**, □, $\delta(^{11}B)$ (mean) −8.7], [8,8-$(PMe_2Ph)_2$-*nido*-8,7-$PtCB_9H_{11}$] [**1**, ○, $\delta(^{11}B)$ (mean) −4.4] and [7,7-$(PMe_2Ph)_2$-*nido*-7-$PtB_{10}H_{12}$] [**4**, △, $\delta(^{11}B)$ (mean) +0.7]. The bottom diagrams are stick representations of the chemical shifts and relative intensities in the ^{11}B NMR spectra, with hatched lines connecting equivalent positions for the four molecules. The top diagram is a plot of $\delta(^{1}H)$ *versus* $\delta(^{11}B)$ for the {BH(*exo*)} units in the four compounds. The solid and the hatched lines drawn have slopes $\delta(^{1}H)$:$\delta(^{11}B)$ of 1:16 and 1:6 respectively, with intercepts in $\delta(^{1}H)$ of +2.65 and +3.65 respectively

metal-to-borane bonding interaction and a square-planar platinum(II) co-ordination sphere (see above).

The ^{11}B shielding of compound **1** may also be compared with those of formally isoelectronic [7,7-$(PMe_2Ph)_2$-7-$PtB_{10}H_{12}$] (**4**, classical *nido* geometry **III**) and [1,1-$(PMe_2Ph)_2$-1,2,3-$PtC_2B_8H_{10}$] (**3**, closed geometry **I**) to examine for intermediacy of electronic behaviour (compare structural discussion above). The closed 1,2,3-platinadicarbaboranes of basic C_{2v} geometry **I** can have either 'compact' or 'expanded' clusters, each with markedly different intracluster dimensions and NMR characteristics.[3] Compound **3** is 'compact', with the {$C_2B_8H_{10}$} unit having *arachno* character,[3] whereas [1,1-$(SEt_2)_2$-1,2,3-$PtC_2B_8H_{10}$] **5** is 'expanded', with the {$C_2B_8H_{10}$} unit having more *nido* character.

Fig. 5 (lower) compares the ^{11}B shielding patterns for compounds **1** and **3**–**5**. There is a sequential transition in ^{11}B shielding behaviour along the structural transition from [$(PMe_2Ph)_2PtB_{10}H_{12}$] **4**, *via* [$(PMe_2Ph)_2PtCB_9H_{11}$] **1** and 'expanded' [$(SEt_2)_2PtC_2B_8H_{10}$] **5**, to 'compact' [$(PMe_2Ph)_2$-$PtC_2B_8H_{10}$] **3**. However, the shielding pattern of compound **1** relates much more closely to that of the conventionally *nido*-structured **4** than to the closed species **3** or **5**. Electronically compound **1** therefore seems much closer to the fully open conventionally *nido*-structured species [7,7-$(PMe_2Ph)_2$-7-$PtB_{10}H_{12}$] **4** than to the closed species **3** and **5** (compare structural discussion above, near Fig. 3). Further support for this derives from the plot of $\delta(^{11}B)$ *versus* $\delta(^{1}H)$ for the BH(*exo*) units of compounds **1** and **3**–**5** [Fig. 5 (upper)]. Compounds **1** and **4** both have a conventional ten-vertex *nido*/*arachno*

Table 5 Measured ^1H, ^{31}P and ^{195}Pt NMR data for [8,8-$(PMe_2Ph)_2$-*nido*-8,7-$PtCB_9H_{11}$] **1** in CD_2Cl_2 solution at 273 K and selected data for compounds **3** and **4** and other comparison species

(*a*) PMe_2Ph data for compound **1**

Assignment	$\delta(^{31}P)^a$	$^1J(^{195}Pt-^{31}P)$/Hz	$\delta(^1H)^b$	$^3J(^{195}Pt-^1H)$/Hz	$^2J(^{31}P-^1H)$/Hz
P(1)	−4.6 (broader)	2722 A	+1.67	24.5	9.5
		2722 B	+1.45	24.5	9.5
P(2)	−9.8 (sharper)	3191 A	+1.95	33.5	11.0
		3191 B	+1.83	28.5	10.5

(*b*) $\{Pt(PMe_2Ph)_2\}$ data for compounds **1**, **3** and **4** and selected non-cluster species

Compound	$\Xi(^{195}Pt)$	$\delta(^{195}Pt)^c$ A	$\delta(^{195}Pt)^c$ B	$^1J(^{195}Pt-^{31}P)$/Hz	$\delta(^{31}P)$	Ref.
4 $\{PtB_{10}\}$	21.379 830	−1978	−942	2534	+1.3	4, 5
1 $\{PtCB_9\}$	21.384 010	−1726	−747	2722	−4.6	This work
				3191	−9.8	
3 $\{PtC_2B_8\}$	21.381 360	−1850	−871	3542	−22.3	3
$[PtMe_2(PMe_2Ph)_2]$	21.397 460	−1098	−119	1820	+5.3	26
$[PtCl_2(PMe_2Ph)_2]$	21.402 710	−853	+127	3548	−16.2	26

^{a} $^2J(^{31}P-^{31}P)$ 28 Hz; the two ^{31}P resonances coalesce at *ca.* 333 K ($C_2D_2Cl_4$ solution, 162 MHz spectrum, 9.4 T); Δν 816 Hz; $\Delta G^‡$ *ca.* 61 kJ mol^{-1}. ^{b} Each of the pairs AA and BB coalesces at 313 ± 5 K ($C_2D_2Cl_4$ solution, 400 MHz spectrum, 9.4 T); Δν 114 and 126 Hz respectively; $\Delta G^‡$ 62.4 and 62.1 kJ mol^{-1} respectively. ^{c} Scale A is relative to Ξ 21.4 MHz (ref. 25) and B to $[PtCl_2(SMe_2)_2]$ as zero (ref. 26).

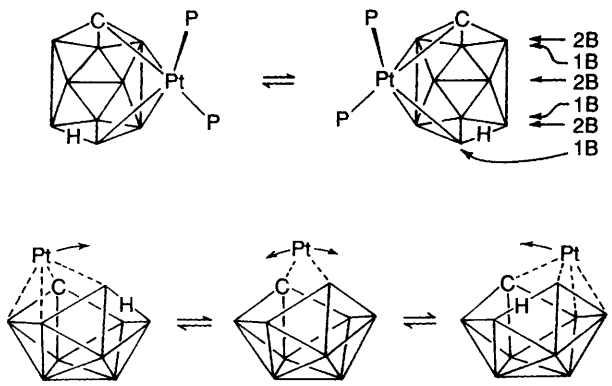

Scheme 1

$\delta(^{11}B):\delta(^1H)$ correlation slope of approximately 16:1 (solid line), whereas the closed species **3** and **5** follow a different correlation trend (hatched line).

It is also of interest to assess the ^{31}P and ^{195}Pt NMR properties of compound **1** for intermediacy between *closo*-structured **3** and *nido*-structured **4** (Table 5). At lower temperature (see below for higher-temperature phenomena), the $^{31}P(2)$ resonance [*trans* to C(7)] is sharper, and the $^{31}P(1)$ resonance [*trans* to B(4)B(9)] is broader, the broadness arising from the $^2J(^{31}P-Pt-^{11}B)$ transoid coupling[28] to $^{11}B(4)$ and $^{11}B(9)$. The larger coupling $^1J(^{195}Pt-^{31}P)$ for P(2) *trans* to more electronegative carbon is also expected.[29] The mean of the two couplings (2956 Hz) is close to the mean of those for compounds **3** and **4** (3038 Hz). In the proton spectrum $^1H-\{^{31}P(selective)\}$ experiments assigned the four inequivalent PMe groups between the P(1) and P(2) positions. In terms of overall ^{195}Pt shielding ranges,[25-27] the $\delta(^{195}Pt)$ values for compounds **1**, **3** and **4** were not particularly different, but nevertheless exhibit somewhat greater shielding than platinum(II) square-planar complexes[27] such as *cis*-$[PtMe_2(PMe_2Ph)_2]$ and *cis*-$[PtCl_2(PMe_2Ph)_2]$. However, suitable comparison data are limited.

Dynamic Behaviour of $[(PMe_2Ph)_2PtCB_9H_{11}]$ **1** *in Solution.*—The above section discusses low-temperature NMR data. At higher temperatures peak coalescences in the ^{11}B, ^{31}P and ^1H NMR spectra occur. The detail shows that these arise from an intramolecular dynamic exchange process. Coalescence

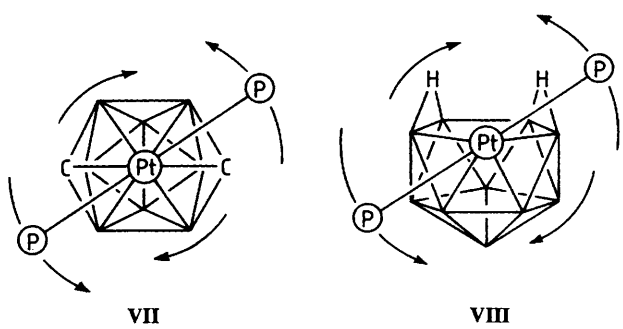

temperatures yield $\Delta G^‡$ values of 60–64 kJ mol^{-1} for 313–340 K, the most accurate being 62.2 ± 1.2 kJ mol^{-1} at 313 K (PMe ^1H resonance coalescence).

Each of the three pairs of ^{11}B NMR resonances from B(1)B(6), B(3)B(11) and B(4)B(10) coalesce, but B(2), B(5) and B(9) are unchanged. This indicates an enantiomeric exchange involving movement of the platinum atom across the formal $\{CB_9H_{10}\}$ 'mirror plane', with a concomitant reverse shift of the bridging hydrogen atom (Scheme 1). The ^{31}P resonance coalescence demonstrates a concomitant exchange of the two phosphines. The pairwise coalescence of the four PMe ^1H resonances, in which each coalescing pair contains one resonance from each PMe_2Ph ligand, discounts a general rotation. This is in contrast to each of the different rotational fluxionalities of compounds **3** (schematic structure **VII**; $\Delta G^‡$ 63 kJ mol^{-1} at 284 K for the 2-Me derivative)[3] or **4** (schematic structure **VIII**; $\Delta G^‡$ 79 kJ mol^{-1} at 344 K),[5] even though the static cluster structure of compound **1** is intermediate between those of **3** and **4** and its $\Delta G^‡$ value is very similar.

Rather, there is a specific shift of the platinum atom across the open face of the $\{CB_9H_{10}\}$ cluster. This is linked with a half-rotation of the $\{(PMe_2Ph)_2\}$ ligand sphere, as indicated in Scheme 2. Scheme 2 shows rotation *via* a Pt–C(7) linkage, although a similar rotation *via* the B(9) end of the subcluster cannot be discounted. The hydrogen atom could move *via* a Pt–H link (Scheme 2), *via* an *endo*-BH(9) [or CH(7)] intermediate, or some intermediate bridging form. The solid-state structure (Fig. 2) shows that the bridging hydrogen is positioned for a ready conversion into an *endo* position on B(9), or for further movement to bind to platinum. In any event its role seems to limit a completely free rotation of the phosphine ligands.

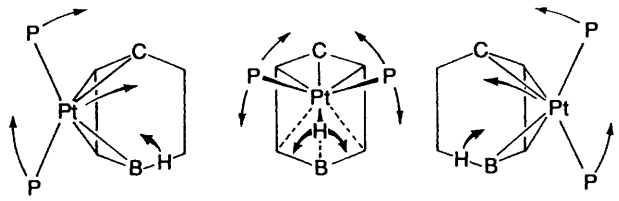

Scheme 2

The cluster geometry of the transition state should also be considered: does the reaction go *via* a *trihapto* linkage (as drawn in Scheme 2) or *via* an intermediate approximating to the closed structure **I** of the isoelectronic compound **3** (as approximately represented in the lower part of Scheme 1)? In this context we note (*a*) that the related *nido*-shaped species [9,9-$(PPh_3)_2$-9,7,8-$RhC_2B_8H_{11}$] (schematic structure **IX**) dynamically equilibrates with its isomer [1-H-1,1-$(PPh_3)_2$-1,2,4-$RhC_2B_8H_{10}$][30] of quasi-closed structure[2] **X** similar to **I**, and (*b*) that another related *nido*-shaped compound, [8,8-$(PPh_3)_2$-8,7-$RhSB_9H_{10}$], exhibits an inter-enantiomeric fluxionality[31] for which there are quasi-isoelectronic $\{MSB_9\}$ models for a closed transition state, *e.g.* [1-(η^5-C_5Me_5)-1,2-$IrSB_9H_9$][32] and [1-(CO)-1,3-$(PPh_3)_2$-1,2-$RhSB_9H_8$].[33]

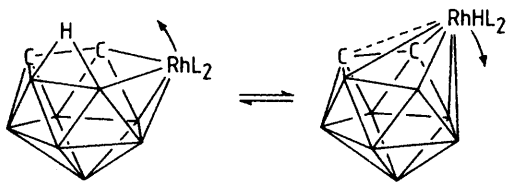

IX X

The fluxionality of compound **1**, involving a half-twist of the $\{(PMe_2Ph)_2\}$ ligand sphere relative to the carborane cluster, appears related to the fluxionality postulated[34] for related quasi-isoelectronic eleven-vertex *nido*-shaped [10,10-$(PMe_3)_2$-10,7,9-$PtC_2B_8H_{10}$] **6**. In compound **6** a carborane subcluster rearrangement as well as a shift of platinum around the open face was proposed.[34] We have not ourselves re-examined **6**, but we have found[8] that its $(PPh_3)_2$ analogue **7** is not fluxional. Rather, the apparent degeneracy observed[34] in the ^{11}B NMR spectrum of **7** (and presumably also for **6**) arises from accidental ^{11}B coincidence among chemically distinct boron atoms, not from exchange.

Experimental

Preparation of Compound **1**.—A sample of $[PtCl_2(PMe_2Ph)_2]$ (137 mg, 250 μmol) was dissolved in CH_2Cl_2 (*ca.* 10 cm^3) under a dinitrogen atmosphere and Cs[*arachno*-6-CB_9H_{14}] (prepared as in ref. 6; 100 mg, 390 μmol) was added in portions with stirring at room temperature, whereupon a yellow colour developed. Stirring was continued for 24 h, the mixture was filtered in air, and silica gel (chromatographic column grade, *ca.* 3 g) added to the filtrate from which the volatile components were then removed *in vacuo*. The resultant solids from the filtrate were then placed on top of a column packed with silica gel (dimensions 2.5 × 15 cm), and subjected to chromatography using C_6H_{12}–CH_2Cl_2 (20:80) as liquid phase to separate three fractions, successively colourless (detected by analytical TLC), yellow (the principal component) and dark yellow. These fractions were reduced in volume to *ca.* 1 cm^3, and individual components were then separated and purified by preparative TLC [silica gel G, layers *ca.* 200 × 200 × 1 mm on glass plates, C_6H_{12}–CH_2Cl_2 (20:80) as liquid phase] to give four products after extraction, evaporation and crystallisation: (*a*) a colourless band (R_f 0.51, detected by UV spectroscopy at 254 nm), recrystallised by diffusion of C_6H_{12} into a solution in C_6H_6 to yield [9,9-$(PMe_2Ph)_2$-*arachno*-9,6-$PtCB_8H_{12}$] **2** as a pale yellow crystalline solid (4 mg, 7 μmol, 3%); (*b*) a colourless band (R_f 0.40, detected at 254 nm) which yielded a pale yellow solid (< 1 mg), as yet unidentified; (*c*) a main lemon-yellow band (R_f 0.29), recrystallised by diffusion of C_6H_{12} into a solution in C_6H_6 to yield [8,8-$(PMe_2Ph)_2$-*nido*-8,7-$PtCB_9H_{11}$] **1** (63 mg) as large orange-yellow crystals, with a second microcrystalline crop (6 mg) being gleaned by evaporation of the mother-liquors (total yield 69 mg, 119 μmol, 46%); (*d*) an orange band (R_f 0.17) which yielded an impure brown-yellow solid (2 mg), as yet unidentified. A similar procedure using $[PtCl_2(PMe_2Ph)_2]$ (175 mg, 320 μmol) and Cs[CB_9H_{14}] (130 mg, 510 μmol) in CH_2Cl_2, (*ca.* 15 cm^3), but with the omission of the column chromatographic stage, resulted in the isolation, by preparative TLC directly from the reaction evaporate, of 123 mg (207 μmol, 64%) of crystalline compound **1**, with only trace quantities (*ca.* 500 μg) of **2** being obtained.

NMR Spectroscopy.—The NMR spectroscopy was performed at *ca.* 2.35 and *ca.* 9.4 T using commercially available JEOL FX-100 and Bruker AM-400 instrumentation respectively. The general techniques, and the techniques of [^{11}B–^{11}B]-COSY,[20,21] [^1H–^1H]-COSY-{^{11}B},[22] and ^1H-{^{11}B} spectroscopy,[35] were essentially as described and illustrated in other recent papers describing NMR work in our laboratories.[24,36–39] Chemical shifts δ are given in ppm positive to high frequency (low field) of Ξ 100 ($SiMe_4$) for ^1H (quoted ± 0.05 ppm), Ξ 40.480 730 (nominally 85% H_3PO_4) for ^{31}P (quoted ± 0.5 ppm), Ξ 21.4 (the Goodfellow frequency)[25] and 21.420 980 {nominally $[PtCl_2(SMe_2)_2]$ in $CDCl_3$}[26] for ^{195}Pt, and Ξ 31.083 971 MHz (nominally $F_3B{\cdot}OEt_2$ in $CDCl_3$)[29] for ^{11}B (quoted ± 0.5 ppm), Ξ being defined as in ref. 40. Spectra were calibrated using solvent resonances as internal secondary standards.

Single-crystal X-Ray Diffraction Analysis.—All crystallographic measurements were made on a Nicolet P3/F diffractometer operating in the ω–2θ scan mode using a standard procedure described elsewhere.[41] The data set was corrected for absorption empirically once the structure had been determined.[42] The structure was determined *via* standard heavy-atom methods and refined by full-matrix least squares using the SHELX program system.[43] All non-hydrogen atoms were refined with anisotropic thermal parameters. The phenyl groups were treated as rigid bodies and refined with idealised hexagonal symmetry. The phenyl and methyl hydrogen atoms were included in calculated positions (C–H 96 pm) and were assigned an overall isotropic parameter. The carbaborane cluster hydrogen atoms were located on a Fourier difference synthesis and were freely refined with individual isotropic thermal parameters. The weighting scheme $w = [\sigma^2(F_o) + g(F_o)^2]^{-1}$ was used in which the parameter g was included in refinement in order to obtain satisfactory agreement analyses. Final non-hydrogen atomic coordinates are given in Table 6.

Crystal data for compound **1**. $C_{17}H_{33}B_9P_2Pt$, M = 591.78, monoclinic, space group $P2_1/n$ (no. 14), a = 1186.8(1), b = 1554.1(2), c = 1344.1(2) pm, β = 95.02(1)°, U = 2.4695(6) nm^3, Z = 4, D_c = 1.59 Mg m^{-3}, μ = 55.74 cm^{-1}, $F(000)$ = 1152.

Data collection. Scan widths 2.0° + α-doublet splitting, scan speeds 2.0–29.3° min^{-1}, 4.0 < 2θ < 50.0°. 4659 Data collected, 3938 with $I > 2.0\sigma(I)$ considered observed, T = 290 K.

Structure refinement. Number of parameters = 295, g = 0.0002, R = 0.0297, R' = 0.0310.

Additional material available from the Cambridge Crystallographic Data Centre comprises thermal parameters and remaining bond lengths and angles.

Acknowledgements

Contribution no. 28 from the Řež–Leeds Anglo–Czech Polyhedral Collaboration (ACPC). We thank the SERC, the

Table 6 Fractional atomic coordinates ($\times 10^4$) for non-hydrogen and cluster hydrogen atoms of [8,8-$(PMe_2Ph)_2$-*nido*-8,7-$PtCB_9H_{11}$] **1** with e.s.d.s in parentheses

Atom	*x*	*y*	*z*	Atom	*x*	*y*	*z*
Pt(8)	978.2(1)	2128.5(1)	1258.4(1)	B(2)	3333(5)	1080(5)	516(5)
P(1)	293(1)	3062(1)	−24(1)	B(3)	2853(5)	1846(4)	1312(5)
P(2)	−183(1)	2605(1)	2386(1)	B(4)	2104(5)	1314(4)	2306(4)
C(11)	−261(5)	2436(4)	−1088(4)	B(5)	2099(6)	207(5)	2007(5)
C(12)	−836(5)	3844(4)	76(5)	B(6)	2725(6)	109(5)	836(5)
C(131)	1424(2)	3732(2)	−409(2)	C(7)	2200(4)	1711(4)	231(4)
C(132)	1519(2)	3956(2)	−1403(2)	B(9)	854(6)	752(4)	1835(5)
C(133)	2388(2)	4501(2)	−1648(2)	B(10)	1269(6)	65(4)	891(5)
C(134)	3162(2)	4821(2)	−898(2)	B(11)	1988(5)	746(4)	−77(5)
C(135)	3067(2)	4597(2)	97(2)	H(1)	4087(13)	706(12)	2310(12)
C(136)	2198(2)	4053(2)	341(2)	H(2)	4143(13)	1180(12)	121(12)
C(21)	−78(6)	2100(5)	3604(4)	H(3)	3406(13)	2626(12)	1408(12)
C(22)	157(6)	3717(4)	2715(5)	H(4)	2136(13)	1561(12)	3070(12)
C(231)	−1671(2)	2565(2)	1989(2)	H(5)	2218(13)	−331(12)	2540(12)
C(232)	−2077(2)	1939(2)	1305(2)	H(6)	2881(13)	−596(12)	670(12)
C(233)	−3223(2)	1915(2)	973(2)	H(7)	2551(13)	2134(12)	−198(13)
C(234)	−3964(2)	2517(2)	1327(2)	H(9)	196(13)	606(12)	2252(12)
C(235)	−3559(2)	3142(2)	2011(2)	H(10)	794(13)	−492(12)	584(12)
C(236)	−2412(2)	3166(2)	2342(2)	H(11)	1928(13)	499(12)	−927(12)
B(1)	3290(5)	853(5)	1787(5)	H(910)	546(13)	620(12)	903(12)

Academy of Sciences of the Czech Republic, the Royal Society, and Borax Research Ltd. for support, and Drs. Dana M. Wagnerová and T. Scott Griffin for helpful cooperation.

References

1 M. Bown, X. L. R. Fontaine, N. N. Greenwood, J. D. Kennedy and M. Thornton-Pett, *J. Chem. Soc., Dalton Trans.*, 1990, 3039.
2 K. Nestor, X. L. R. Fontaine, N. N. Greenwood, J. D. Kennedy, J. Plešek, B. Štíbr and M. Thornton-Pett, *Inorg. Chem.*, 1989, **28**, 2219.
3 J. D. Kennedy, B. Štíbr, M. Thornton-Pett and T. Jelínek, *Inorg. Chem.*, 1991, **30**, 4481; J. D. Kennedy, K. Nestor, B. Štíbr, M. Thornton-Pett and G. S. A. Zammitt, *J. Organomet. Chem.*, 1992, **477**, Cl; J. D. Kennedy, B. Štíbr, T. Jelínek, X. L. R. Fontaine and M. Thornton-Pett, *Collect. Czech. Chem. Commun.*, 1993, in the press.
4 S. K. Boocock, N. N. Greenwood, J. D. Kennedy, W. S. McDonald and J. Staves, *J. Chem. Soc., Dalton Trans.*, 1981, 2573.
5 S. K. Boocock, N. N. Greenwood and J. D. Kennedy, *J. Chem. Soc., Chem. Commun.*, 1980, 305.
6 B. Štíbr, T. Jelínek, J. Plešek and S. Heřmánek, *J. Chem. Soc., Chem. Commun.*, 1987, 963.
7 C. K. Johnson, ORTEP II, Report ORNL-5738, Oak Ridge National Laboratory, TN, 1976.
8 J. H. Jones, B. Štíbr, M. Thornton-Pett and J. D. Kennedy, to be submitted for publication; J. H. Jones, results presented to the Seventh International Meeting on Boron Chemistry, (IMEBORON VII), Torun', Poland, July–August 1990, Abstract CA14.
9 M. A. Beckett, J. E. Crook, N. N. Greenwood and J. D. Kennedy, *J. Chem. Soc., Dalton Trans.*, 1986, 1879.
10 Faridoon, O. Ni Dhubhghaill, T. R. Spalding, G. Ferguson, X. L. R. Fontaine and J. D. Kennedy, *J. Chem. Soc., Dalton Trans.*, 1989, 1657.
11 J. Bould, N. N. Greenwood and J. D. Kennedy, *J. Chem. Soc., Dalton Trans.*, 1984, 2477.
12 See, for example, J. D. Kennedy, *Prog. Inorg. Chem.*, 1986, **34**, 272, 278 and 348ff.
13 R. E. Williams, *Inorg. Chem.*, 1971, **10**, 210; *Adv. Inorg. Chem. Radiochem.*, 1976, **18**, 67.
14 K. Wade, *Chem. Commun.*, 1971, 792; *Adv. Inorg. Chem. Radiochem.*, 1976, **18**, 1.
15 K. Baše, B. Štíbr, J. Dolanský and J. Duben, *Collect. Czech. Chem. Commun.*, 1981, **46**, 2479; J. Plešek, B. Štíbr, X. L. R. Fontaine, T. Jelínek, S. Heřmánek, J. D. Kennedy and M. Thornton-Pett, *Inorg. Chem.*, 1993, to be submitted for publication.
16 K. Nestor, B. Štíbr, T. Jelínek, K. Baše, X. L. R. Fontaine, J. D. Kennedy and M. Thornton-Pett, *J. Chem. Soc., Dalton Trans.*, 1990, 2887.
17 J. D. Kennedy and B. Wrackmeyer, *Magn. Reson. Chem.*, 1980, **38**, 529.
18 J. Bould, J. E. Crook, J. D. Kennedy and M. Thornton-Pett, *Inorg. Chim. Acta*, 1993, **203**, 193.
19 B. Štíbr and J. D. Kennedy, results communicated to the Eleventh Meeting of the Silicon, Tin, Germanium, and Lead Discussion Group of the Royal Society of Chemistry, London, 21st April, 1989, Communication P3.
20 T. Venable, W. C. Hutton and R. N. Grimes, *J. Am. Chem. Soc.*, 1984, **106**, 29.
21 D. Reed, *J. Chem. Res.*, 1984, (*S*) 198.
22 X. L. R. Fontaine and J. D. Kennedy, *J. Chem. Soc., Chem. Commun.*, 1986, 779.
23 M. A. Beckett and J. D. Kennedy, *J. Chem. Soc., Chem. Commun.*, 1983, 575.
24 M. Bown, X. L. R. Fontaine and J. D. Kennedy, *J. Chem. Soc., Dalton Trans.*, 1988, 1467.
25 See, for example, R. G. Goodfellow in *Multinuclear NMR*, ed. J. Mason, Plenum, London and New York, 1987, ch. 10, pp. 521–561 and refs. therein.
26 W. McFarlane, *J. Chem. Soc., Dalton Trans.*, 1974, 324.
27 J. D. Kennedy, W. McFarlane, R. J. Puddephatt and P. J. Thompson, *J. Chem. Soc., Dalton Trans.*, 1976, 874.
28 J. D. Kennedy and J. Staves, *Z. Naturforsch., Teil B*, 1979, **34**, 808.
29 See, for example, J. D. Kennedy in *Multinuclear NMR*, ed. J. Mason, Plenum, London and New York, 1987, ch. 8, pp. 221–254 and refs. therein.
30 C. W. Jung and M. F. Hawthorne, *J. Am. Chem. Soc.*, 1980, **102**, 3024.
31 G. Ferguson, M. C. Jennings, A. J. Lough, S. Coughlan, T. R. Spalding, J. D. Kennedy, X. L. R. Fontaine and B. Štíbr, *J. Chem. Soc., Chem. Commun.*, 1990, 891.
32 K. Nestor, X. L. R. Fontaine, N. N. Greenwood, J. D. Kennedy and M. Thornton-Pett, *J. Chem. Soc., Dalton Trans.*, 1991, 2657.
33 S. Coughlan, T. R. Spalding, G. Ferguson, J. Gallagher, A. J. Lough, X. L. R. Fontaine, J. D. Kennedy and B. Štíbr, *J. Chem. Soc., Dalton Trans.*, 1992, 2865.
34 M. Green, J. L. Spencer and F. G. A. Stone, *J. Chem. Soc., Dalton Trans.*, 1979, 1679.
35 J. D. Kennedy and N. N. Greenwood, *Inorg. Chim. Acta*, 1980, **38**, 529.
36 X. L. R. Fontaine and J. D. Kennedy, *J. Chem. Soc., Dalton Trans.*, 1987, 1573.
37 M. A. Beckett, M. Bown, X. L. R. Fontaine, N. N. Greenwood, J. D. Kennedy and M. Thornton-Pett, *J. Chem. Soc., Dalton Trans.*, 1988, 1969.
38 M. Bown, J. Plešek, K. Baše, B. Štíbr, X. L. R. Fontaine, N. N. Greenwood and J. D. Kennedy, *Magn. Reson. Chem.*, 1989, **27**, 947.
39 G. Ferguson, J. D. Kennedy, X. L. R. Fontaine, Faridoon and T. R. Spalding, *J. Chem. Soc., Dalton Trans.*, 1988, 2555; X. L. R. Fontaine, J. D. Kennedy, M. McGrath and T. R. Spalding, *Magn. Reson. Chem.*, 1991, **89**, 711.
40 W. McFarlane, *Proc. R. Soc. London, Ser. A*, 1965, **306**, 185.
41 A. Modinos and P. Woodward, *J. Chem. Soc., Dalton Trans.*, 1974, 2065.
42 N. Walker and D. Stuart, *Acta Crystallogr., Sect. A*, 1983, **39**, 2065.
43 G. M. Sheldrick, SHELX 76, Program System for X-Ray Structure Determination, University of Cambridge, 1976.

Received 5th August 1992; *Paper* 2/04235E